Geochemistry Geophysics Geosystems G3
AN ELECTRONIC JOURNAL OF THE EARTH SCIENCES
Published by AGU and the Geochemical Society

Article
Volume 7, Number 9
7 September 2006
Q09P16, doi:10.1029/2005GC001156
ISSN: 1525-2027

Glacial deep water carbonate chemistry inferred from foraminiferal Mg/Ca: A case study from the western tropical Atlantic

Jennifer Fehrenbacher, Pamela A. Martin, and Gidon Eshel

Department of Geophysical Sciences, University of Chicago, 5734 South Ellis Avenue, Chicago, Illinois 60637, USA (jsf1@uchicago.edu)

[1] We explore using changes in planktonic foraminiferal Mg/Ca with water depth in a single region to infer relative changes in deep water carbonate chemistry. The Mg/Ca ratio in foraminiferal calcite is quantitatively lowered by dissolution. We exploit this dissolution effect to generate a profile of carbonate ion concentration (CO_3^{2-}) for the deep waters of the tropical Atlantic during the Last Glacial Maximum. We generated Mg/Ca data for three species, *G. ruber*, *G. sacculifer*, and *N. dutertrei*, from three cores located along a depth transect (2.8 to 4.0 km) on the Ceara Rise in the western equatorial Atlantic. We attribute lower Mg/Ca in glacial intervals from the shallow core to changes in sea surface temperature (SST). The even lower glacial Mg/Ca values in the deeper cores are attributed to dissolution and are used to reconstruct a paleo-CO_3^{2-} profile. Our down core Mg/Ca data for *G. ruber* and *G. sacculifer* confirm that these species are more resistant to Mg loss due to dissolution than *N. dutertrei*. The greater susceptibility of *N. dutertrei*'s Mg content to dissolution limits the utility of this species in thermocline temperature reconstructions to cores above the lysocline but, significant to this study, makes *N. dutertrei* useful in quantifying changes in deep water CO_3^{2-}. Our paleo-CO_3^{2-} reconstruction based on *N. dutertrei* suggests the Last Glacial Maximum CO_3^{2-} gradient in the Atlantic was much steeper than today, implying that the boundary between deepwater masses in the Atlantic was shallower during the Last Glacial Maximum. Our results suggest comparison of Mg/Ca from multiple cores from one region could similarly provide constraints on changes in carbonate chemistry in other basins and other time periods.

Components: 11,139 words, 11 figures, 3 tables.

Keywords: Last Glacial Maximum; Mg/Ca; paleocarbonate ion; planktonic foraminifera.

Index Terms: 4271 Oceanography: General: Physical and chemical properties of seawater; 4924 Paleoceanography: Geochemical tracers; 4926 Paleoceanography: Glacial.

Received 30 September 2005; **Revised** 8 March 2006; **Accepted** 8 June 2006; **Published** 7 September 2006.

Fehrenbacher, J., P. A. Martin, and G. Eshel (2006), Glacial deep water carbonate chemistry inferred from foraminiferal Mg/Ca: A case study from the western tropical Atlantic, *Geochem. Geophys. Geosyst.*, *7*, Q09P16, doi:10.1029/2005GC001156.

Theme: Development of the Foraminiferal Mg/Ca Proxy for Paleoceanography
Guest Editor: Pamela Martin

1. Introduction

[2] Deepwater carbonate ion concentration, CO_3^{2-}, can be used to infer changes in the carbon cycle and ocean circulation over time. Interpretation of the changes is complicated because deep water CO_3^{2-} is affected by the physical and biological processes occurring at sites of deepwater formation, glacial-interglacial changes in carbon inventories, and the circulation of the deepwater masses (for a review, see *Archer et al.* [2000]). Nonetheless, accurate reconstructions of temporal variations in both the absolute and relative changes in CO_3^{2-} can be used to test hypotheses about the causes of lower CO_2 levels during the Last Glacial Maximum (LGM) and previous glacial periods as well as track the reorganization of deepwater masses [*Broecker*, 1982; *Archer and Maier-Reimer*, 1994; *Sanyal et al.*, 1995; *Moore et al.*, 2000; *Sigman and Boyle*, 2000; *Barker et al.*, 2004; *Marchitto et al.*, 2002].

[3] Several different methods have been proposed for reconstructing deepwater carbonate ion concentration, and the related parameters carbonate dissolution and pH. Many of the proxies rely on some aspect of foraminiferal shell changes, including changes in species abundance, fragmentation, and shell crystallinity [*Volbers and Henrich*, 2002, 2004; *Bassinot et al.*, 2004; *Pfuhl and Shackleton*, 2004]. One method that has received considerable attention is the use of foraminiferal shell mass as a proxy for dissolution [*Lohmann*, 1995; *Broecker and Clark*, 2001a, 2001b, 2003]. Results from the initial *Broecker and Clark* [2001a] study indicate a steeply decreasing carbonate ion gradient in the Atlantic and a slight increase in carbonate ion concentration with increasing water depth in the Pacific. However, subsequent studies have indicated that the shell mass proxy can be biased by environmental factors affecting initial shell mass (e.g., optimum growth conditions [*de Villiers*, 2004] or carbonate ion concentration (or saturation state) [*Spero et al.*, 1997; *Barker and Elderfield*, 2002]). A reevaluation of the initial study led *Broecker and Clark* [2003] to the conclusion that the deep Atlantic CO_3^{2-} gradient may not have been substantially steeper, rather may have nearly uniformly shifted to lower values over the depth range studied. A study by *Anderson and Archer* [2002], using modern foraminiferal assemblages as a proxy for reconstructing sea surface temperature (SST) and CO_3^{2-}, yielded results in sharp contrast to Broecker and Clark's original study. *Anderson and Archer* [2002] suggested dissolution intensity in the Atlantic decreased slightly with increasing water depth in the deep during the LGM [*Anderson and Archer*, 2002]. Other studies also yield differing estimates of glacial CO_3^{2-} highlighting the need for multiple proxies of past CO_3^{2-} [e.g., *Barker et al.*, 2004].

[4] We propose a new method for reconstructing carbonate ion concentration using the Mg/Ca ratio of planktonic foraminifera. Many studies have utilized foraminiferal Mg/Ca to reconstruct sea surface temperature changes [*Hastings et al.*, 1998; *Lea et al.*, 1999; *Elderfield and Ganssen*, 2000; *Anand et al.*, 2003; *McKenna and Prell*, 2004; *Pak et al.*, 2004; *McConnell and Thunell*, 2005]. Core top studies indicate shell Mg/Ca is also subject to dissolution on the seafloor [*Brown and Elderfield*, 1996; *Rosenthal and Lohmann*, 2002; *de Villiers*, 2003]. A significant factor in controlling dissolution on the seafloor is the carbonate saturation state of deep waters, the relative difference between the in situ carbonate ion concentration ($[CO_3^{2-}]_{in\ situ}$) and the saturation carbonate ion concentration ($[CO_3^{2-}]_{sat}$), the latter primarily controlled by depth/pressure in the deep sea. A comprehensive study of foraminifera collected from sediment cores yielded a large calibration data set, including Pacific and Atlantic samples, which demonstrated that Mg/Ca decreased quantitatively with decreases in bottom water carbonate saturation. This study established calibrations for *G. ruber*, *G. sacculifer*, and *N. dutertrei* that included a correction term for the effect of dissolution on the Mg/Ca ratio [*Dekens et al.*, 2002]. Here, we use a Mg-derived estimate of glacial-SST and the core top calibration data of *Dekens et al.* [2002] to reconstruct a deepwater carbonate ion concentration gradient for the LGM.

2. Methods

2.1. Approach and Samples

[5] Our approach quantitatively compares the Mg/Ca ratio of foraminifera shells recovered from a set of three cores from a depth transect (2.8–4.0 km) along the Ceara Rise in the western equatorial Atlantic (~5N 43W; Table 1). We chose this location (1) because previous studies have suggested that there has been a reorganization of deepwater masses in the western tropical Atlantic during the LGM [*Duplessy et al.*, 1988;

Table 1. Core and Core Locations Used in This Study

Core	Latitude	Longitude	Water Depth, m
KNR110 82	4°20.2′N	43°29.2′W	2816
KNR110 66	4°33.8′N	43°22.9′W	3547
KNR110 50	4°51.9′N	43°12.3′W	3995

Curry and Oppo, 2005], implying a large change in CO_3^{2-}, and (2) for direct comparison to *Broecker and Clark*'s [2001a] reconstruction. Many of the shells used in our study were the same shells weighed by *Broecker and Clark* [2001a, 2001b] in their initial study of shell masses on the Ceara Rise. The three cores are regionally closely spaced (Figure 1) and contain foraminifera that probably calcified under the same sea surface conditions; therefore the shells have recorded the same sea surface temperature in their Mg/Ca ratio and should have similar Mg/Ca ratios as they fall to the seafloor. The shells settle on the seafloor at different depths where they experience different intensities of dissolution due to differences in the bottom water carbonate ion saturation state, which is controlled primarily by water depth (the pressure effect on solubility) and water mass chemistry. We neglect the effect of pore water dissolution driven by respiration CO_2. We assume that samples from the shallowest core undergo the least amount of dissolution and that the down core (interglacial-glacial) changes in Mg/Ca in the shallowest core are due to change in temperature only (but later revisit the consequences of this assumption). We use the shallowest core (KNR110 82, 2.8 km) to reconstruct an LGM SST. We then use the LGM SST to reconstruct glacial to interglacial changes in carbonate ion concentration by comparing the residual differences in Mg/Ca at different water depths through time.

2.2. Sample Preparation and Analyses

[6] We analyzed Mg/Ca in three species of planktonic foraminifera, *G. ruber*, *G. sacculifer*, and *N. dutertrei*. Thirty to sixty *G. ruber* shells and approximately fifty shells of *G. sacculifer* (without the sac-like final chamber) and *N. dutertrei* were picked from the 250–355 μm size fraction. With smaller sample size (less than 40 shells), 0.35–0.45 mg of shells were gently crushed between glass plates and placed into one vial. In intervals with high enough abundances to yield enough shells for duplicate measurements, approximately 0.7–0.9 mg of shells were gently crushed, homogenized with a dry brush and separated into two vials. Samples were cleaned of contaminating phases using a multistep trace metal cleaning protocol including reductive cleaning with buffered hydrazine [*Boyle and Keigwin*, 1985], a protocol previously tested for samples targeted for Mg/Ca analyses [*Martin and Lea*, 2002]. Beginning with cracking and loading of the picked foraminifera, samples were handled in a clean room (Class 100). Sample cleaning was done in a side-ventilated class 100 flow hood.

[7] The cleaned samples were dissolved in a spiked acid solution and analyzed by HR ICP-MS in D. Lea's Laboratory at UCSB using a method originally developed for quadrapole ICP-MS [*Lea and Martin*, 1996], modified for the magnetic sector instrument (HR ICP-MS). Samples were analyzed for a suite of minor and trace constituents, including Al, Fe and Na to assess the potential for contaminant phases from sediments (Al and Fe) and from cleaning (Na). We excluded samples with anomalously high Al/Ca, Fe/Ca or Na/Ca (greater than two orders of magnitude higher than mean values) from the data set (18 out of 287 samples). Long-term reproducibility is estimated as ±2%. The average

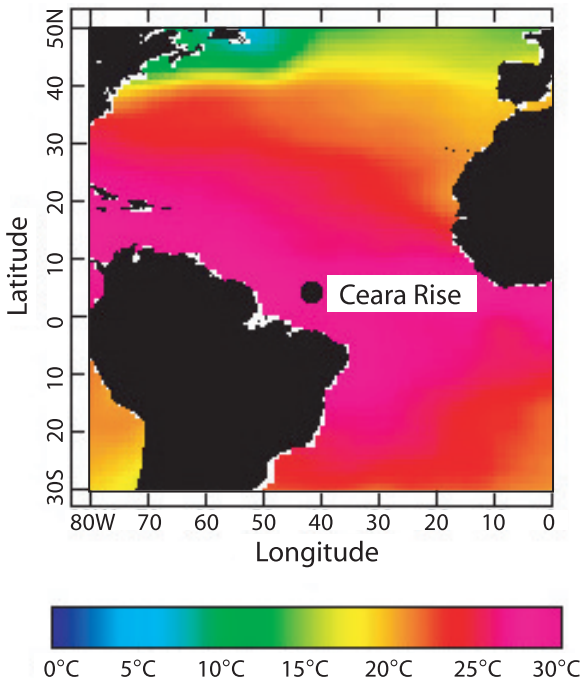

Figure 1. Map of core locations. Modern sea surface temperature is shown to illustrate the warm tropical surface waters at the location above the core sites. Sea surface temperature from *Levitus and Boyer* [1994].

coefficient of variation is 0.12 mmol/mol for 123 sample pairs.

3. Planktonic Mg/Ca Results

3.1. Species Offsets

[8] We analyzed three species of planktonic foraminifera in cores from three depths, yielding a total of nine short glacial-interglacial records (Figures 2 and 3). In all three cores (Figures 2a, 2b, and 2c), *G. ruber* and *G. sacculifer* have Mg/Ca values similar to one another during the Holocene and the last glacial, with slightly higher *G. ruber* Mg/Ca during the Holocene and slightly lower *G. ruber* Mg/Ca during the glacial intervals of the middepth and deep cores. Note that the depth of the LGM, identified by the $\delta^{18}O$ variation (Figure 2) and radiocarbon dates (Figure 3), varies for each of the cores [*Curry et al.*, 1988]. *N. dutertrei* have substantially lower Mg/Ca values (~30–50%) than the other species in all three cores. Previous studies have noted that differences among the Mg/Ca ratios for the different species are at least partly reflective of differences in their calcification and depth habitats [*Anand et al.*, 2003]. *G. ruber* and *G. sacculifer* are spinose species that live in the mixed layer. *G. sacculifer* has a slightly deeper depth habitat (20 m). *N. dutertrei* is a nonspinose thermocline dwelling species that lives in a wide range of depths and is often associated with the chlorophyll maximum [*Fairbanks and Wiebe*, 1980; *Fairbanks et al.*, 1982].

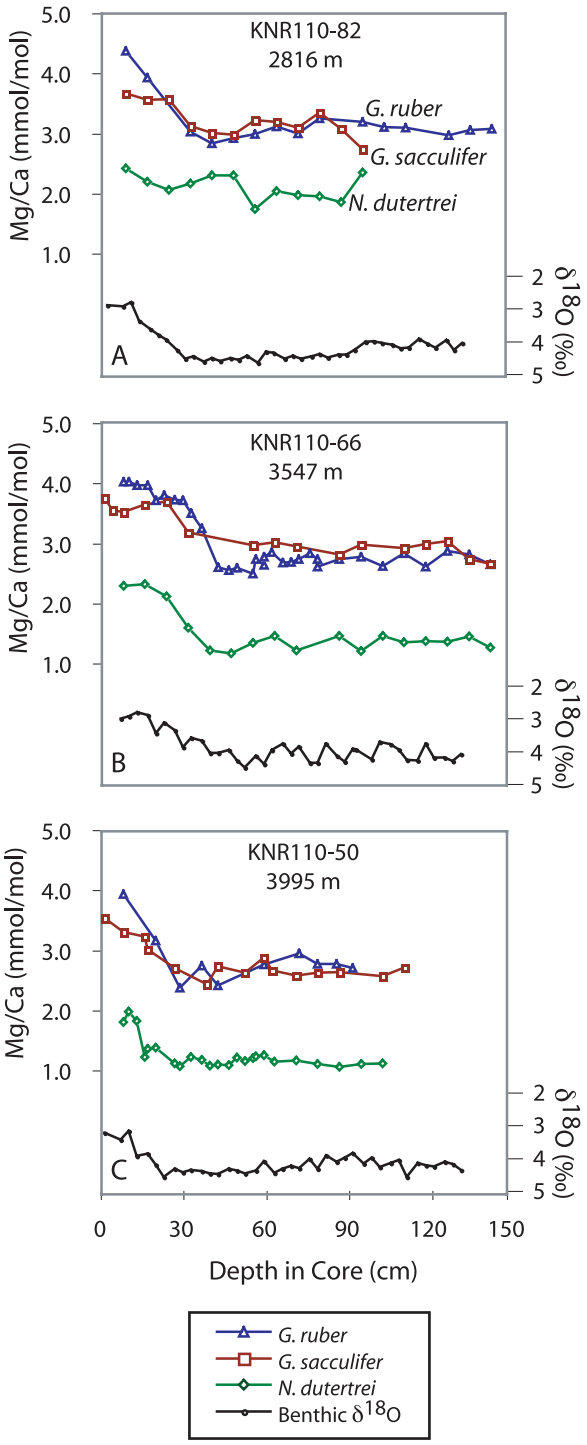

3.2. Variation in Mg/Ca With Water Depth and Down Core

3.2.1. *G. ruber*

[9] Comparison of the *G. ruber* Mg/Ca from all three cores (Figure 3a, Table 2) shows that the Mg/Ca ratio decreases slightly with increasing water depth; however, the difference in Mg/Ca between

Figure 2. Plots of Mg/Ca versus depth in core, grouped by core depth. Each plot shows Mg/Ca for three planktonic species. Benthic $\delta^{18}O$ (black line) are shown for stratigraphy [*Curry et al.*, 1988]. (a) In the shallow core, *G. ruber* (blue) and *G. sacculifer* (red) show a small offset in their core top values but similar decreasing values in Mg/Ca down core. Mg/Ca for *N. dutertrei* (green) is persistently lower than *G. ruber* and *G. sacculifer*. (b) In the middepth core, *G. ruber* and *G. sacculifer* Mg/Ca again record similar values throughout the glacial-interglacial record. There is a larger offset in the *N. dutertrei* Mg/Ca values from the other two species during the glacial than in the shallower core. (c) In the deep core there are limited data for *G. ruber* and *G. sacculifer* due to dissolution. As in the other cores, the data show similar Mg/Ca for these two surface-dwelling species. *N. dutertrei* Mg/Ca show an offset from the other two species but a smaller glacial-interglacial signal than in the middepth core. All three species in all three cores show a decrease in the Mg/Ca ratio from the Holocene to the Last Glacial Maximum.

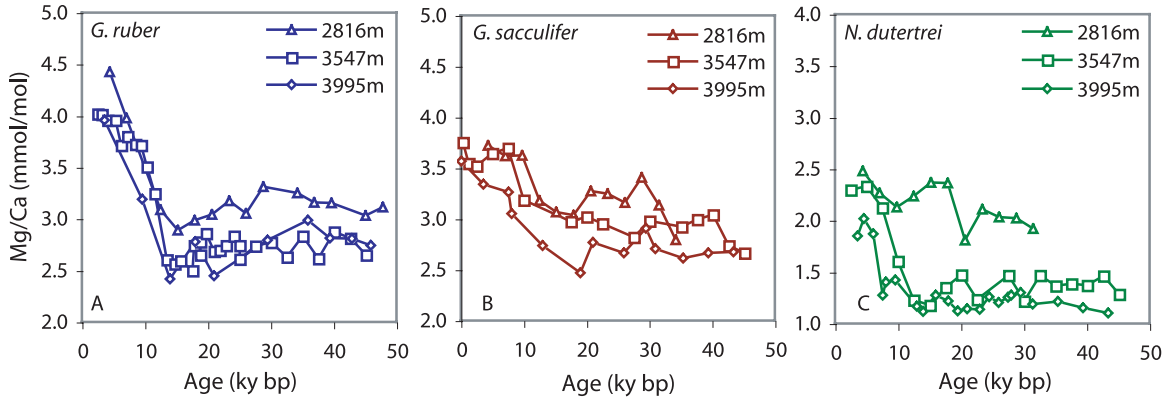

Figure 3. Plots of Mg/Ca versus age, grouped by species. Each plot shows Mg/Ca for three core depths. There is a glacial-interglacial decrease in Mg/Ca values for all three species in all three cores. (a) *G. ruber* show a small offset in the Mg/Ca between the shallowest core (triangles) and the middepth core (squares). There are limited data for *G. ruber* in the deep core (diamonds). (b) *G. sacculifer* show nearly identical values for all three core depths throughout the entire record. (c) *N. dutertrei* record similar Mg/Ca values in the shallow and middepth cores during the Holocene, but during the Last Glacial, *N. dutertrei* Mg/Ca values are nearly identical in the middepth and deep cores.

the shallow and deep core (i.e., the decrease in Mg/Ca with increased water depth) is small relative to the down core glacial-interglacial change (i.e., the Mg/Ca change attributed to temperature change). For example, in Holocene samples, the Mg/Ca of *G. ruber* ranges from 4.4 mmol/mol in the shallow core (2.8 km) to 3.9 mmol/mol in the deep core (4.0 km), or ~9% per km, whereas the glacial-interglacial decrease in the shallow core is 31%. The glacial-interglacial Mg/Ca is comparable in the deep core (34%).

3.2.2. *G. sacculifer*

[10] For *G. sacculifer* (Figure 3b, Table 2), there is only a slight offset in Mg/Ca between the Holocene samples from the shallow and deep core and this offset is small relative to the down core glacial-interglacial changes in each core. In Holocene samples, the Mg/Ca of *G. sacculifer* ranges from 3.7 mmol/mol in the shallow core (2.8 km) to 3.5 mmol/mol in the deep core (4.0 km). This translates to a 4% decrease in Mg/Ca per km relative to a glacial-interglacial change of 15% in the shallow core. The glacial-interglacial Mg/Ca change is larger in the deep core (26%), and thus the decrease in Mg/Ca with water depth is slightly larger during the glacial. Comparison of LGM samples from the shallow and deep cores shows a 0.5 mmol/mol (14%) decrease in Mg/Ca per km.

3.2.3. *N. dutertrei*

[11] There is a much larger decrease in Mg/Ca with increasing water depth for *N. dutertrei* (Figure 3c, Table 2) than for *G. ruber* or *G. sacculifer*. Comparison of the core top values shows that the decrease in Mg/Ca between the shallow and deep cores is comparable to the down core glacial-interglacial Mg/Ca decrease in the shallow core. The Mg/Ca of *N. dutertrei* from the shallowest intervals of the three different cores ranges from 2.5 mmol/mol (2.8 km) to 1.9 mmol/mol (4.0 km), which translates to an average decrease of 0.5

Table 2. Holocene and LGM Mg/Ca, Reconstructed SST Using KNR110-82, 2.8 km

Species	Mg/Ca, mmol/mol		SST, °C			Change in Mg/Ca	
	Holocene	LGM	Modern (Levitus)	Holocene Mg-Derived	LGM Mg-Derived	Per km Change in-Depth Holocene/LGM	Down Core Glacial-Interglacial
G. ruber	4.426	2.068	27.4	29.2	24.6	9%/13%	31%
G. sacculifer	3.724	2.074	27.4	27.5	25.5	4%/14%	14%
N. dutertrei	2.480	2.142	35.8 (75 m)	25.8	22.3	22%/39%	16%

mmol/mol (22%) Mg/Ca per km. The down core glacial-interglacial change in Mg/Ca in the shallow core is 16%. The most striking feature of the entire data set is the glacial-interglacial change in the *N. dutertrei* Mg/Ca from the middepth core (3.5 km). During the Holocene, *N. dutertrei* Mg/Ca values are nearly the same in the shallow and middepth cores. During the glacial, *N. dutertrei* Mg/Ca are nearly identical in the iddepth and deep cores. Also notable is the large offset in the Mg/Ca between the shallow and deep cores during the last glacial. During the LGM, the Mg/Ca of *N. dutertrei* decreased by an average of ~37% per km.

4. Discussion

4.1. Relative Sensitivities of the Mg/Ca to Temperature and Dissolution

[12] Down core Mg/Ca variations in our records reflect temporal changes in both temperature and dissolution. Differences in the amplitude of these Mg/Ca variations among the nine records suggests that there are differences in the sensitivity of the Mg-content of different species to temperature and dissolution, consistent with conclusions based on modern calibration data [*Dekens et al.*, 2002]. The broad similarity of the *G. ruber* and *G. sacculifer* over a range of water depths, relative to the changes recorded by the *N. dutertrei*, is general confirmation that the two surface dwelling species have similar temperature and dissolution sensitivities (Figure 2; see also equations (1) and (2) below). *G. ruber* exhibit a distinct offset in Mg/Ca with increasing water depth, not seen as clearly in the *G. sacculifer* data, suggesting that the *G. ruber* shells are somewhat more sensitive to preservation changes than *G. sacculifer*. With both species, the temporal Mg/Ca changes appear to be dominated by temperature.

[13] The *N. dutertrei* Mg/Ca variations are distinct from the surface dwelling species in (1) their absolute value (lower); (2) the small amplitude of the glacial-interglacial in the shallowest (best-preserved) core; and (3) the large decreases in Mg/Ca with increasing water depth among the Holocene samples (Figure 2). The lower Mg/Ca value of the *N. dutertrei* relative to *G. ruber* and *G. sacculifer* is at least partially reflective of their depth habitat in the water column, as mentioned above. The small amplitude of the glacial-interglacial Mg/Ca change in the shallowest core is consistent with the weak temperature sensitivity of *N. dutertrei* Mg/Ca (~4.5% per degree versus ~8% per degree for *G. ruber*). In contrast, the large decreases in *N. dutertrei* Mg/Ca with increasing water depth are indicative of a high sensitivity of the shell Mg to dissolution.

[14] The apparent high sensitivity of *N. dutertrei* Mg loss to dissolution intensity implies that this species should be the most sensitive of the three species to past changes in deep water carbonate saturation state. Consistent with this, *N. dutertrei* show the most dramatic changes in the amplitude of glacial-interglacial Mg/Ca with increasing water depth (Figure 3c). In the Holocene, Mg/Ca are similar in the shallow and middepth cores consistent with being bathed in the same water mass. Our hypothesis is that the similar *N. dutertrei* Mg/Ca in the middepth and deep cores in the LGM intervals reflects a shift in water masses, such that the middepth and deep cores were in the same water mass during the LGM. In addition, we hypothesize that the larger LGM differences in *N. dutertrei* Mg/Ca between the shallow and deep core are due to a steeper dissolution gradient on the Ceara Rise during the LGM also most likely resulting from a change in the configuration of deepwater masses. In the next sections, we quantify the changes in temperature and dissolution to evaluate this hypothesis and the relative utility of the three species in reconstructing ΔCO_3^{2-}.

4.2. Temperature Reconstructions From Core KNR110 82 (2.8 km): Holocene and LGM

[15] To isolate the relative changes in saturation state, we must first correct for the portion of the temporal Mg/Ca change resulting from the glacial-interglacial temperature change. We use the Mg/Ca data from the *shallowest core* (2.8 km) to reconstruct the temperatures (sea surface and thermocline) during the Holocene and LGM using equations from *Dekens et al.* [2002]:

G. ruber

$$\mathrm{Mg/Ca} = 0.37 \exp 0.08\left[\mathrm{SST} + 0.042\left(\Delta CO_3^{2-}\right)\right] \quad (1)$$

G. sacculifer

$$\mathrm{Mg/Ca} = 0.31 \exp 0.084\left[\mathrm{SST} + 0.048\left(\Delta CO_3^{2-}\right)\right] \quad (2)$$

N. dutertrei

$$\mathrm{Mg/Ca} = 0.42 \exp 0.05\left[\mathrm{SST} + 0.222\left(\Delta CO_3^{2-}\right)\right] \quad (3)$$

where $\Delta CO_3^{2-} = [CO_3^{2-}]_{\text{in situ}} - [CO_3^{2-}]_{\text{sat}}$, i.e., ΔCO_3^{2-} is a representation of the saturation state at a given core site. A slightly expanded *G. ruber* calibration data set yielded a small change from the published *G. ruber* equation (equation (1) above). We use the modern ΔCO_3^{2-}, 44 μmol/kg,

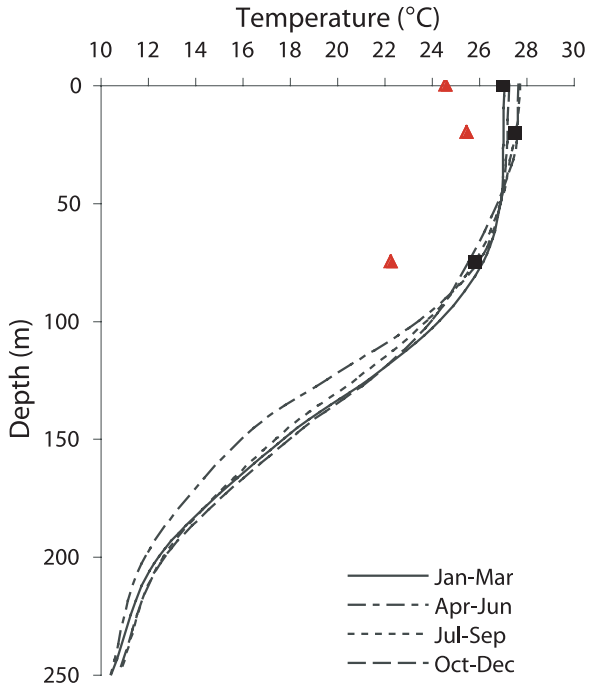

Figure 4. Modern temperature profile (dashed and solid lines) and the Mg-derived Holocene (black squares) and Last Glacial Maximum (red triangles) sea surface temperatures (SST) at the Ceara Rise. The average glacial SST derived from *G. ruber* and *G. sacculifer* is ~2.4°C lower than modern. The temperature reconstructed from *N. dutertrei* is ~3.5°C lower than modern. As noted in the text, the modern SST in this figure derived from *G. ruber* was obtained using the Mg/Ca from *Dekens et al.* [2002].

for all depth intervals in the core (calculated by *Dekens et al.* [2002] using the Program Developed for CO_2 System Calculations by E. Lewis and D. W. R. Wallace). This approach is comparable to other studies that calculate temperatures using a single calibration equation, either with or without a correction for water depth. We discuss the implications of this assumption for reconstructing carbonate ion concentrations in the discussion below.

[16] For the Holocene (our shallowest samples), we obtain a Mg-derived SST of 29.2°C (±1.2) for *G. ruber*, higher than the mean annual SST at the Ceara Rise of 27.4°C [*Levitus and Boyer*, 1994]. The sample used to calculate the *G. ruber* SST is from 8 cm in the core. We suspect that the higher SST reconstructed from this interval may reflect a Holocene maximum. Using a shallower sample from this core, *Dekens et al.* [2002] data yield a SST of 27.4. For *G. sacculifer* we obtain a SST of 27.5°C (±1.4). The reconstructed SST from *G. sacculifer* is comparable to today's mean annual temperatures at the Ceara Rise of 27.4°C [*Levitus and Boyer*, 1994] (Figure 4). We obtain a thermocline temperature of 25.8°C (±1.6) from *N. dutertrei*, a deeper dwelling species associated with the thermocline. The reconstructed thermocline temperature is also comparable to today's mean annual thermocline temperature of 25.8°C at 75 m depth [*Levitus and Boyer*, 1994] (Figure 4). The equation we use to generate thermocline SST was calibrated by *Dekens et al.* [2002] using temperatures found at 75 m depth.

[17] For the LGM we obtain an estimated SST of 24.6°C for *G. ruber* and 25.5°C for *G. sacculifer* and an LGM thermocline temperature of 22.4°C for *N. dutertrei* using the shallowest core. The average glacial-interglacial change in SST is 2.4°C (relative to *Levitus and Boyer* [1994]) and for the thermocline the glacial-interglacial change in temperature is 3.4°C. The change in glacial-interglacial SST is within the range of other LGM tropical temperature reconstructions [*Mix et al.*, 1999; *Guilderson et al.*, 2001; *Rosenthal and Lohmann*, 2002; *Trend-Staid and Prell*, 2002; *Rosell-Melé et al.*, 2004]. The glacial-interglacial change in thermocline temperature is also within the range of a glacial-interglacial temperature estimate derived from comparison of $\delta^{18}O$ of planktonic/benthic foraminifera at other low-latitude Atlantic sites [*Slowey and Curry*, 1995].

4.3. Reconstructing ΔCO_3^{2-} Using Planktonic Mg/Ca: Comparison of the Modern Gradient Reconstructed From Three Species

[18] To reconstruct the deep-sea carbonate ion gradient, we use the Mg/Ca from the middepth and deep cores and the same equations (equations (1)–(3)) [after *Dekens et al.*, 2002]. Now, we substitute the Mg-derived temperatures from the shallowest core (calculated above) and solve the equation for ΔCO_3^{2-}. To compare the temperature and dissolution effects it is useful to slightly rearrange the equations so that the exponential change in each parameter can be compared directly:

G. ruber

$$Mg/Ca = 0.37 \exp\left[0.08(SST) + 0.0034\left(\Delta CO_3^{2-}\right)\right] \quad (4)$$

G. sacculifer

$$Mg/Ca = 0.31 \exp\left[0.084(SST) + 0.0040\left(\Delta CO_3^{2-}\right)\right] \quad (5)$$

N. dutertrei

$$Mg/Ca = 0.42 \exp\left[0.05(SST) + 0.0111\left(\Delta CO_3^{2-}\right)\right] \quad (6)$$

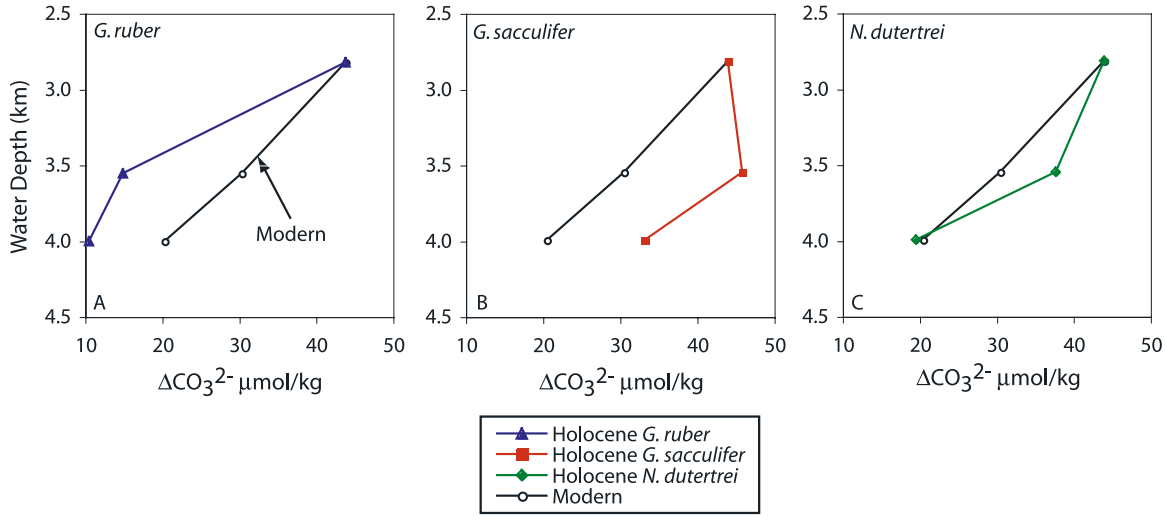

Figure 5. Actual and reconstructed modern ΔCO_3^{2-} gradient versus water depth. The ΔCO_3^{2-} gradient is defined as $\Delta CO_3^{2-} = [CO_3^{2-}]_{sat} - [CO_3^{2-}]_{in\ situ}$ and reconstructed using Mg/Ca from three planktonic species. The actual gradient (black) reconstructed using GEOSECS data (see text) is shown for comparison. (a) The ΔCO_3^{2-} gradient reconstructed from *G. ruber* (blue) is steeper relative to the shallow core and yields lower values than the modern (black) in the middepth and deep cores. (b) The ΔCO_3^{2-} gradient reconstructed from *G. sacculifer* (red) is not as steep as the modern gradient and yields higher values than the modern in the middepth and deep cores. (c) The ΔCO_3^{2-} gradient reconstructed from *N. dutertrei* (green) accurately reflects the modern gradient and yields values similar to the modern in the middepth and deep cores.

The ΔCO_3^{2-} effect on *G. ruber* and *G. sacculifer* Mg/Ca in the equations is small in comparison to *N. dutertrei.* For example, the calibration equations imply that a 10 μmol/mol decrease in ΔCO_3^{2-} lowers the Mg/Ca of *G. ruber* by ~3% and *N. dutertrei* by ~10%; to put this change in perspective, the range of $[CO_3^{2-}]_{in\ situ}$ in modern deep Atlantic water masses is ~40 μmol/mol. The difference in the sensitivity to dissolution is qualitatively consistent with our down core data, noticeable as a larger offset in *N. dutertrei* Mg/Ca with increasing water depth relative to the other two species and larger amplitude of the glacial-interglacial change in *N. dutertrei* in the middepth core at 3.5 km.

[19] We first compute carbonate ion concentration for Holocene samples of each species to reconstruct a modern vertical profile of carbonate ion concentration for comparison with the actual modern vertical profile of carbonate ion concentration (Figure 5). The modern profile was produced using ΔCO_3^{2-} at each core depth calculated by *Dekens et al.* [2002] using data from WOCE and input into the Program Developed for CO_2 System Calculations by E. Lewis and D.W. R. Wallace. In the modern deep Atlantic Ocean the carbonate ion concentration is quite uniform over a large depth range, ~112 μmol/kg [*Broecker and Sutherland*, 2000]. The concentration decreases at depth due to the transition between North Atlantic Deep Water (NADW) and Antarctic Bottom Water (AABW), which has a lower carbonate ion concentration of ~84 μmol/kg [*Broecker and Sutherland*, 2000]. This transition is deep in the western tropical Atlantic. For example, at 4.5 km, 500 meters deeper than our deepest core, the carbonate ion concentration is ~100 μmol/kg, reflective of the mixing zone of NADW and AABW.

[20] *G. ruber* (Figure 5a) and *G. sacculifer* (Figure 5b) do not accurately record the modern carbonate ion gradient. *G. ruber* substantially overestimates the modern decrease in ΔCO_3^{2-} with depth whereas *G. sacculifer* substantially underestimates the decrease in ΔCO_3^{2-} with depth. Differences between the actual and the reconstructed carbonate ion gradient may reflect inaccuracies in the calibration equations (which we explore further below). However, the error in reconstructing the modern gradient is not surprising given the relatively low sensitivity of the Mg/Ca content of these species to dissolution change (3–4% per 10 μmol/kg change in ΔCO_3^{2-}, ~60–65% less sensitive to dissolution than *N. dutertrei*). Given the relative insensitivity to dissolution, small differences in *G. ruber* and *G. sacculifer* Mg/Ca will be interpreted as large changes in ΔCO_3^{2-}. For

example, a 4% change in Mg/Ca, comparable to the reproducibility of replicate samples in this data set, would translate to a ~10 μmol/kg change in ΔCO_3^{2-}. Along the 1.2 km water depth change in our cores from the Ceara Rise from the shallow to deep core we would expect to see only a ~7% loss in Mg/Ca in both *G. ruber* and *G. sacculifer* associated with the pressure effect on carbonate saturation state. For comparison, *N. dutertrei* equations predict a ~20% Mg/Ca loss due to pressure related saturation changes over the same depth range.

[21] In contrast to the two surface-dwelling species, Holocene-age *N. dutertrei* yields a carbonate saturation profile similar to the modern (Figure 5c), reflecting a good fit of our core top data with the calibration equations. Note that samples from the cores we use in this study were among samples used in the global calibration set. Because of the more accurate modern reconstruction and greater sensitivity of the Mg-content to carbonate saturation state, we focus on the *N. dutertrei* to reconstruct the carbonate ion concentration gradient for the LGM. The greater sensitivity of the Mg-content of *N. dutertrei* to dissolution along with the small change in Mg/Ca from temperature changes makes it easier to isolate the dissolution signal. An added advantage to using *N. dutertrei* is that shells are structurally resistant to dissolution; that is, they remain whole and identifiable in sediment samples that have experienced fairly intense dissolution and in samples in which many other species are highly fragmented and even entirely dissolved [*Berger*, 1970].

4.4. A Detailed Examination of the *N. dutertrei* Calibration Equation

4.4.1. Examination of the Model Equation for Reconstructions of ΔCO_3^{2-}

[22] Paleo-reconstructions are dependent on the accuracy of the calibration equation based on modern data; therefore we closely examined the original calibration equation for *N. dutertrei.* In *Dekens et al.* [2002] equations relating Mg/Ca, temperature and ΔCO_3^{2-} were derived following a model in which temperature was predicted from ln(Mg/Ca) and ΔCO_3^{2-} (i.e., temperature was chosen as the dependent variable in equations (1)–(3) above). Our primary interest is in using *N. dutertrei* Mg/Ca variations to reconstruct of ΔCO_3^{2-}. Toward this end, we developed an alternative calibration equation for *N. dutertrei* using the original data set. Here, we choose to fit the Mg/Ca data from the calibration set using ΔCO_3^{2-} and temperature (at 75 m) as independent variables. The model equation follows the form:

$$\ln(Mg/Ca) = a + \alpha T + \beta \Delta CO_3^{2-} \quad (7)$$

This approach to interpreting the calibration data, which minimizes the residual in ln(Mg/Ca), is consistent with the physical model in which shell Mg/Ca is controlled by temperature (here, using temperature at 75 m) and dissolution (saturation state). We use the full data set published by *Dekens et al.* [2002] to obtain the equation

N. dutertrei

$$Mg/Ca = 0.50 \ \exp\left[0.044(SST) + 0.0109\left(\Delta CO_3^{2-}\right)\right] \quad (8)$$

This equation is similar to the equations obtained for *N. dutertrei* by a multilinear regression of the calibration data choosing either temperature or carbonate ion as the dependent variable. A similar exercise using the *G. ruber* and *G. sacculifer* data yielded substantially different equations, most likely due to a combination of the much weaker (shell-Mg) dissolution response and smaller calibration data sets for these other species. Given the smaller response of *G. ruber* and *G. sacculifer* shell Mg/Ca to dissolution, we do not explore the calibrations for these species further in this study.

[23] The modern gradient in ΔCO_3^{2-} reconstructed using the revised equation above, shown in Figure 6, is within <1 μmol/kg of the gradient reconstructed from equation (3); the glacial-interglacial temperature change are also slightly larger (e.g., 4.2°C versus 3.4°C). The modern temperature for 75 m calculated from *N. dutertrei* from the shallowest core using the modern ΔCO_3^{2-} as an estimate of glacial ΔCO_3^{2-} is 25.5°C; the glacial temperature change is 21.3°C. We use the revised equation (equation (8)) in the reconstruction below. First, however, we explore estimates of the error in ΔCO_3^{2-} predicted from the new equation.

4.4.2. Estimation of Error

[24] The coefficients relating Mg/Ca, ΔCO_3^{2-} and temperature are pivotal to reconstructing ΔCO_3^{2-}. Consequently, determining their most probable numerical values, as well as the range of these values, is important. We evaluate the "optimal" values and their reasonable ranges using two independent methods, a traditional parametric evaluation and a nonparametric Monte Carlo procedure.

[25] We first estimate the range of coefficients in the calibration equations using the traditional para-

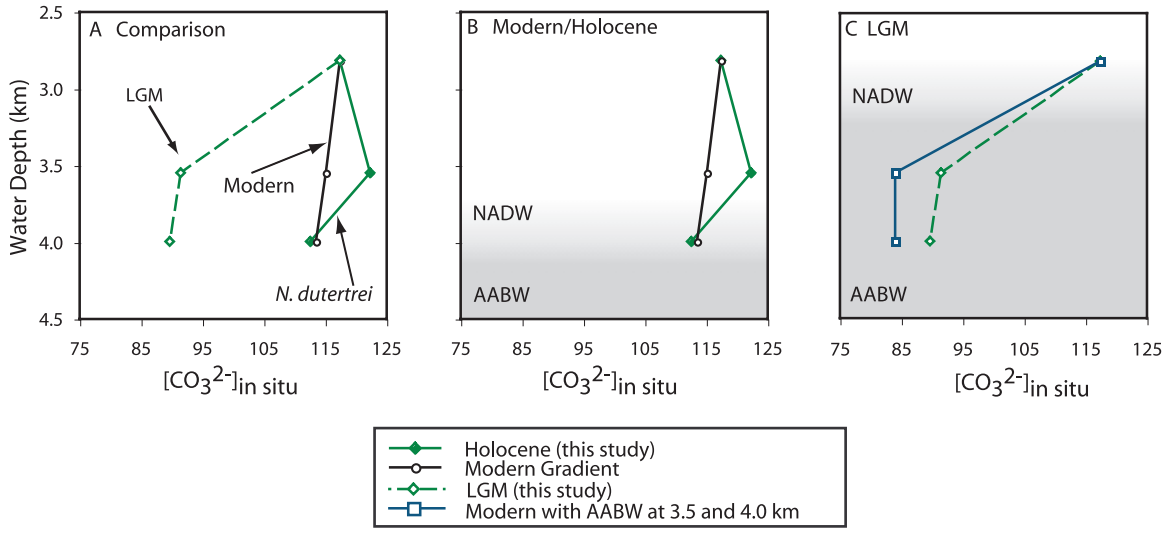

Figure 6. Holocene and LGM reconstructed $[CO_3^{2-}]_{in\ situ}$ gradients versus depth; reconstructed using *N. dutertrei*. To evaluate hypothesized changes in water mass structure, we now plot the $[CO_3^{2-}]_{in\ situ}$ rather than the ΔCO_3^{2-} (an indicator of saturation state). Our values are still calculated assuming no temporal change in the shallowest core. (a) Comparison of the modern $[CO_3^{2-}]_{in\ situ}$ (black solid line) with the reconstructed Holocene (green solid line) and LGM (green dashed line) $[CO_3^{2-}]_{in\ situ}$. The glacial $[CO_3^{2-}]_{in\ situ}$ gradient is steeper than the modern and reconstructed Holocene gradients and has lower values in the middepth and deep cores. (b) The modern (black solid line) and reconstructed (green solid line) $[CO_3^{2-}]_{in\ situ}$ gradients relative to the transition between NADW and AABW in the modern deep Atlantic. The modern $[CO_3^{2-}]_{in\ situ}$ gradient decreases at depth due to mixing between the two water masses; NADW has a carbonate ion concentration of ~112 μmol/kg, and AABW has a carbonate ion concentration of ~84 μmol/kg, an ~30 μmol/kg difference. (c) Comparison of the reconstructed $[CO_3^{2-}]_{in\ situ}$ gradient (green dashed line) and a representation of what the modern $[CO_3^{2-}]_{in\ situ}$ gradient would look like if AABW shoaled to 3.5 km or shallower (blue solid line).

metric evaluation of the 95% confidence intervals on the least squares coefficients,

$$\beta - \frac{t_{sig}^{N-2} s_y}{\sqrt{s_{xx}}} \le \beta^{true} \le \beta + \frac{t_{sig}^{N-2} s_y}{\sqrt{s_{xx}}},$$

where the vector beta contains the estimated linear model coefficients, N-2 is the number of degrees of freedom of the fit (we assume each core is an independent realization, so that N is the number of cores), s_y is the sample based estimate of the standard deviation of the predictand and s_{xx} is the sample based estimate of the standard deviation of the centered (zero-mean) predictors. These estimates are reported in Table 3.

[26] The second method we use to estimate the ranges of the regression coefficients employs a nonparametric, Monte Carlo procedure in which the regression coefficients are calculated with N_w samples withheld (i.e., excluded from the analysis, which therefore comprises N minus N_w samples). We report here the results of separate applications of the methods, with N_w = 2, 3, 4 and 5, each repeated 10,000 times (Monte Carlo realizations).

[27] Since the results with N_w = 4 or 5 are essentially indistinguishable, we combine them to a Monte Carlo population size of 20,000 to calculate the range of coefficients. Histograms of the coefficients computed in all of those 20,000 Monte Carlo realizations show the distribution of a (the pre-exponential constant), alpha (the exponential constant on the temperature) and beta (the exponential constant on the ΔCO_3^{2-}) (Figure 7).

[28] We also use the Monte Carlo simulation to estimate the error on our ΔCO_3^{2-} estimate (Figure 8). First, we examined the residual in ln(Mg/Ca) alternately using only temperature (Fig-

Table 3. Range of Coefficients in the Calibration Equations

SST Only		ΔCO_3^{2-} Only		Full Model		
a	α	a	β	a	α	β
0.447	0.0374	1.248	0.0097	0.462	0.0401	0.0101
0.546	0.0463	1.303	0.0113	0.501	0.0438	0.0109
0.667	0.0552	1.359	0.0131	0.543	0.0474	0.0117

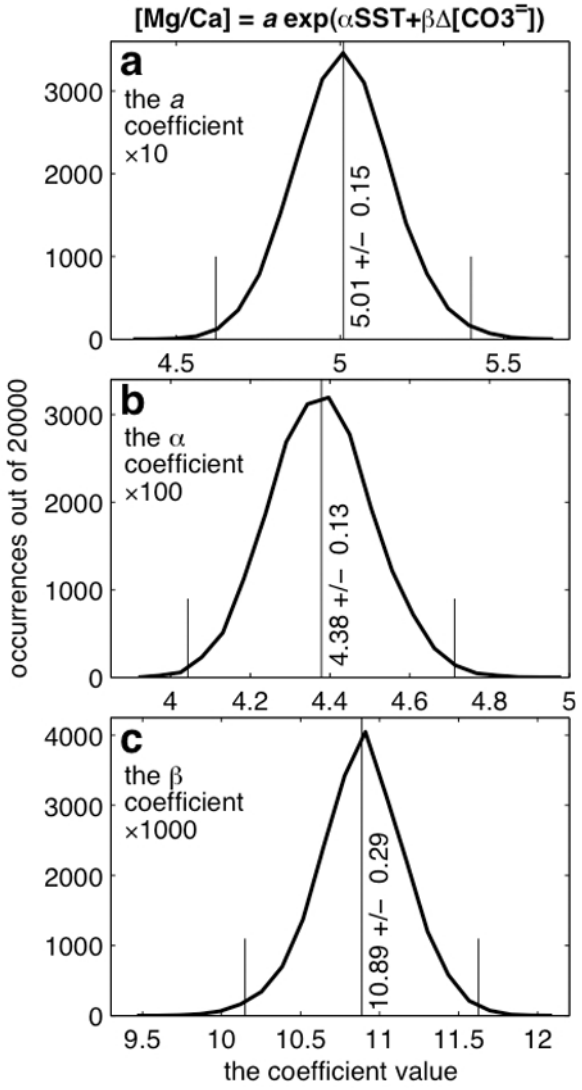

Figure 7. Histograms (finite approximations to the probability density functions) of the optimized coefficients obtained for NMC = 10,000 Monte Carlo realizations described in the previous caption. Figures 7a, 7b, and 7c show coefficients a, α, and β, respectively. In each panel, the NMC values obtained are partitioned into equal-width bins, and the curves show the number of realization (out of 10,000) that fall into a given bin (the coefficient value range of which can be read on the horizontal axis). The mean of each of the three populations is shown as a full vertical bar, while the ±2.58 standard deviation range about the mean (encompassing 99% of the population) is shown by the shorter vertical bars. The numerical values of the mean and standard deviation are shown near the mean bar.

ure 8, top, first panel), only ΔCO_3^{2-} (Figure 8, top, second panel), and both temperature and ΔCO_3^{2-} to predict Mg/Ca (Figure 8, top, third through sixth panels). The multiple estimates of the Mg/Ca using both temperature and ΔCO_3^{2-} follow the scheme of

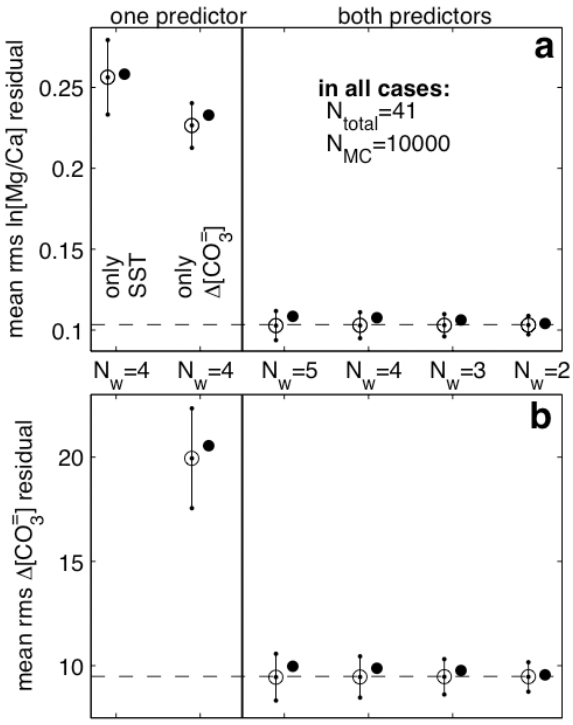

Figure 8. Range of skills of the calibration equations. In Figure 8a the equation to which the data are fitted is $\ln([Mg/Ca]) = \ln(a) + \alpha SST + \beta\Delta[CO_3^{=}]$. In each of the N_{MC} = 10,000 Monte Carlo realizations, randomly chosen N_w = 2, 3, 4, and 5 of the N_{total} = 41 available samples are withheld, and the regression analysis is performed with only $N_{total} - N_w$ samples. The RMS residual means (i.e., $\frac{1}{N_{MC}}\sum_{1}^{N_{MC}}\frac{r^T r}{N_{total}-N_w}$ with $r = \ln([Mg/Ca]^{observed} - \ln([Mg/Ca])^{predicted}$) resulting from hindcasting ln([Mg/Ca]) with each N_w value using the optimized coefficients (a, α, β) are shown by the empty circles to the right of the thick vertical bar. The ±2.58 standard deviation range (encompassing 99% of the population) is shown for each N_w by the vertical spread bars. The results shown to the left of the thick vertical bar use the same notation and symbols, but are based on a single predictor, i.e., from left to right, $\ln([Mg/Ca]) = \ln(a) + \alpha SST$ and $\ln([Mg/Ca]) = \ln(a) + \beta\Delta[CO_3^{=}]$. The horizontal dashed line shows the RMS ln([Mg/Ca]) residual for the full data set (i.e., the calculations analogous to the one done in each of the Monte Carlo realizations, but which use the full data set, with 41 samples). The filled circles show the results of cross-validation, in which the equation, with the optimized coefficients obtained using the deficient sample set (excluding the N_w withheld ones), is used to "forecast" the values of the N_w withheld samples. In Figure 8b the equation is rearranged, $\Delta[CO_3^{=}] = \frac{1}{\beta}[\ln([Mg/Ca]) - \ln(a) - \alpha SST$, and used with the coefficients optimized earlier to predict delta carbonate, using the same symbols as in Figure 8a.

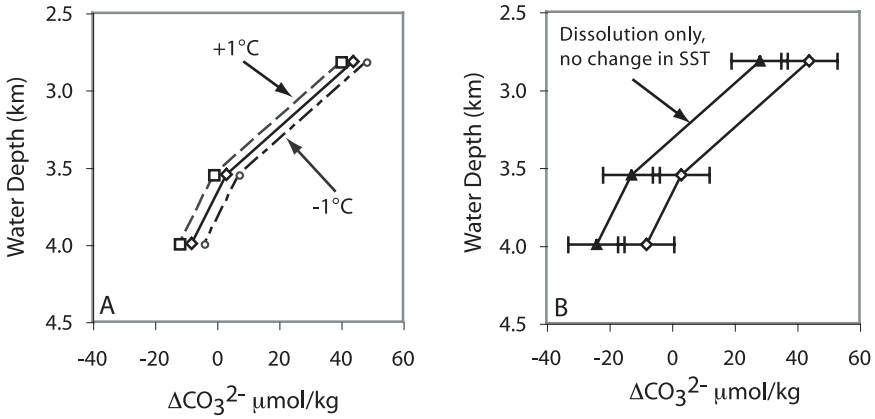

Figure 9. Illustration of potential error on the reconstructed ΔCO_3^{2-} profile. The ΔCO_3^{2-} gradient is defined as $\Delta CO_3^{2-} = [CO_3^{2-}]_{sat} - [CO_3^{2-}]_{in\ situ}$ and reconstructed using Mg/Ca from *N. dutertrei*. (a) We illustrate how the reconstructed ΔCO_3^{2-} gradient shifts if the reconstructed Last Glacial Maximum sea surface temperature is not accurate due to dissolution in the shallow core (yielding lower reconstructed temperatures) or by enhanced preservation in the shallow core (yielding higher reconstructed temperatures). (b) If the entire glacial-interglacial Mg/Ca change in the shallowest core were due entirely to dissolution (no change in SST glacial-interglacial), the curve would shift ~15 μmol/kg to the left. Results demonstrate the shape and magnitude of the curve does not change. This illustrates that the gradient we obtain gives us an absolute change in $[CO_3^{2-}]$ between cores and that any error in our sea surface temperature reconstruction does not change the gradient, only its placement in "carbonate ion space."

randomly removing 2–5 samples from the calibration set. Using only ΔCO_3^{2-} yields lower residuals in ln(Mg/Ca), i.e., the mismatch between predicted and actual Mg/Ca values in the calibration data set, than only using temperature in to predict Mg/Ca supporting our earlier conclusion that ΔCO_3^{2-} has a more significant effect on Mg/Ca than temperature. Using both temperature and ΔCO_3^{2-} significantly reduces the residuals in ln(Mg/Ca).

[29] The results of the Monte Carlo simulations can also be cast in terms of the residual in ΔCO_3^{2-} to estimate an error for our reconstructions. We estimate are error in ΔCO_3^{2-} reconstructed from this calibration data set to be ~9 μmol/kg. The range on our estimated error (the error bars in the lower panel, Figure 8) is ~7 to 11 μmol/kg implying a relatively tightly constrained estimate. The estimate of the residual in ΔCO_3^{2-} based on hindcasting (i.e., based on the difference between the Mg/Ca values predicted from the regression equation and the actual Mg/Ca used to generate the regression equation; open circles in Figure 8) is comparable to the estimate of the residual in ΔCO_3^{2-} obtained by cross-validation (i.e., based on the difference between the Mg/Ca predicted from the regression equation and the actual Mg/Ca value of samples excluded from the regression equation in each Monte Carlo simulation; filled circles in Figure 8).

4.5. Glacial Reconstructions of ΔCO_3^{2-}

[30] Rearranging equation (8) above, we calculate changes in the ΔCO_3^{2-} concentration with increased depth using the measured Mg/Ca of *N. dutertrei* and the glacial temperature in the shallowest core. We correct this for the depth effect on saturation (i.e., subtract the $[CO_3^{2}]_{sat}$) and generate a $[CO_3^{2-}]_{in\ situ}$ profile (Figure 6a). Between the shallow and middepth core we find a decrease in the carbonate ion concentration of 30μmol/kg and a negligible difference between the middepth and deep cores (~3 μmol/kg). The glacial $[CO_3^{2-}]_{in\ situ}$ gradient over the entire depth range is ~25 μmol/kg steeper than the modern gradient.

[31] By assuming there has been no change in the carbonate ion content in the shallow core, our gradient is reconstructed relative to the modern carbonate chemistry at the shallow site. The assumption that there has been no change in ΔCO_3^{2-} at the site of the 2.8 km core, and thus that the entire glacial-interglacial Mg/Ca change is due to temperature, affects the absolute values of the reconstructed carbonate ion concentration but does not change the amplitude of the gradients between each of the cores. For example, if a portion of the *N. dutertrei* Mg/Ca decrease were due to lower carbonate ion concentration (more corrosive waters) and the glacial temperature were only 2°C (versus 3°C) lower, the carbonate ion reconstruc-

tion would be uniformly shifted ~4 μmol/kg lower (Figure 9a).

[32] The Mg-derived ΔCO_3^{2-} between 3.5 and 4.0 km, ~3 μmol/kg, is less than the pressure effect on calcite solubility (which is within the error of reconstruction between 3.5 and 4.0 km) and, as we proposed earlier, suggests that those two cores were in the same water mass during the LGM. The difference between the middepth and shallow core, 30 μmol/kg, is steeper than would be expected solely from the pressure effect on calcite and suggests that these cores were bathed in different water masses during the LGM. Next, we explore the consequences of a simple upward shift of low CO_3^{2-} bottom water with a chemical composition similar to modern AABW (Figure 6c).

[33] In the modern deep Atlantic Ocean the primary process that governs the concentration of carbonate ion is the mixing of the two dominant deep water masses, nutrient depleted, low pCO_2/high CO_3^{2-} North Atlantic Deep Water (NADW) and the more nutrient enriched, relatively high pCO_2/low CO_3^{2-} Antarctic Bottom Water (AABW). The carbonate ion concentration is set in these waters by processes governing the nutrient content of the surface waters in the source regions as well as the extent of equilibration of these sinking water masses with the carbon dioxide concentration of the atmosphere. In the equatorial deep Atlantic, and throughout much of the rest of the deep Atlantic, the $[CO_3^{2-}]_{in\ situ}$ content is relatively uniform (~112 μmol/kg).

[34] Today, the deepest site in our study is bathed in a mixture of mostly NADW influenced by mixing with AABW. Pure (end-member) AABW has a carbonate ion concentration of ~84 μmol/kg. Using a $[CO_3^{2-}]_{in\ situ}$ value of 84 μmol/kg, representing modern AABW, and bathing both the 3.5 and 4.0 km cores in modern AABW, we obtain a gradient nearly identical to the one reconstructed for the LGM (Figure 6c). This illustrates that our glacial gradient could be explained by a simple change in the configuration of deepwater masses without any change in the end-member carbonate chemistry. However, it is likely that our shallowest site (as we discuss below) is not bathed in a pure end-member NADW, but a mixture of NADW and AABW [*Curry and Oppo*, 2005]. This implies a larger contrast between glacial NADW and AABW than their modern counterparts. A shallower lysocline may be due to the penetration of AABW further northward in the glacial Atlantic at shallower water depths. Many studies present evidence of changes in Atlantic thermohaline circulation (THC) during the last glacial [*Boyle and Keigwin*, 1987; *Duplessy et al.*, 1988; *Labeyrie et al.*, 1992; *Adkins et al.*, 1997, 2002; *Martin and Lea*, 1998; *Broecker and Clark*, 2001a]. Our results are also broadly consistent with the glacial water mass configurations derived from $\delta^{13}C$ that imply the presence of a southern ocean water source penetrating further into the North Atlantic during the LGM [*Curry and Oppo*, 2005]. We also note similarities in our reconstruction with the findings of *Barker et al.* [2004] and *Marchitto et al.* [2002], who also find a decrease in carbonate ion concentration in the North Atlantic during the LGM. Both studies indicate an increased presence of a southern ocean water source penetrating further into the North Atlantic during the LGM.

[35] Although our gradient can be explained entirely by a shift in water masses with compositions identical to modern NADW and AABW, we cannot rule out concomitant shifts toward higher or lower carbonate ion concentration in both end-member compositions nor can we rule out that our shallowest site is bathed in a mixture of glacial deep water masses rather than a pure end-member. However, glacial-interglacial temperature estimates from our shallow core as well as estimates from other tropical reconstructions place some constraints on absolute changes in carbonate ion concentration. We estimate a ~4°C glacial-interglacial shift in temperature (~75 m). It is unlikely that the temperatures were warmer than present temperatures during the glacial; thus, if the entire *N. dutertrei* Mg/Ca change that we attribute to temperature were actually due to dissolution, the Mg/Ca data would imply uniformly a ~15 μmol/kg decrease in $[CO_3^{2-}]_{in\ situ}$ (Figure 9b).

[36] Alternatively, if glacial temperatures were even lower than our temperature reconstructions, then the Mg/Ca data would imply that the $[CO_3^{2-}]_{in\ situ}$ was uniformly higher by 4 μmol/kg for every degree we have underestimated glacial cooling (Figure 9a). That the shells from glacial intervals in all three cores appear more dissolved makes it unlikely that the $[CO_3^{2-}]_{in\ situ}$ higher. Rather, the visual evidence of dissolution (Figure 10) suggests that part of the glacial-interglacial Mg/Ca change in the *N. dutertrei* at the shallowest site is due to dissolution and the entire curve might be shifted to somewhat lower carbonate ion concentrations. This shift is unlikely to be too large, however, as our thermocline temperature estimates are comparable to other

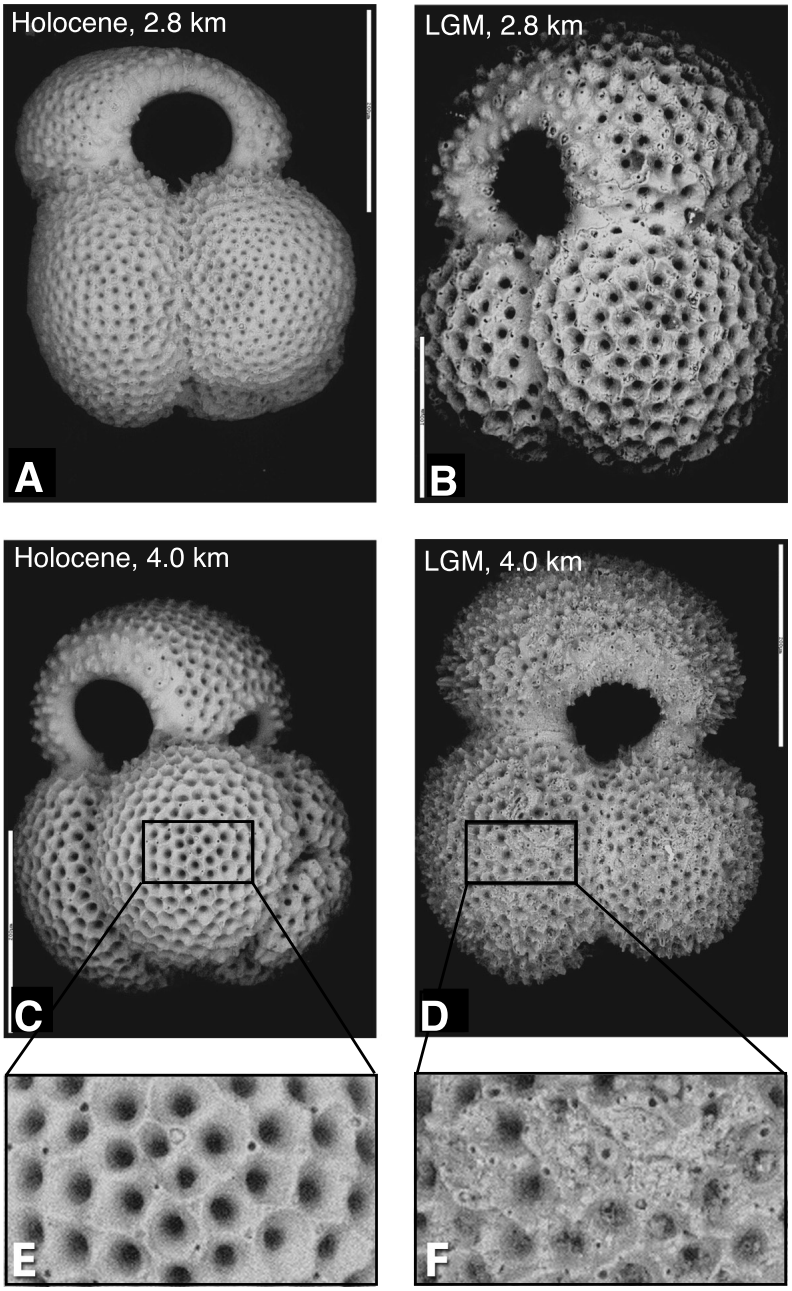

Figure 10. Scanning electron micrograph (SEM) pictures of *G. ruber* from (a and c) core top samples and (b and d) LGM samples from the shallow core (KNR110 82, 2.8 km) and deep core (KNR110 50, 4.0 km). *G. ruber* from the 2.8 km core (Figure 10a) is relatively well preserved, while *G. ruber* from the 4.0 km core shows some evidence of dissolution, including increased pore sizes and some slight pitting (shown in the enlarged SEM (Figure 10e) detailing the boxed area of Figure 10c). *G. ruber* from the LGM samples (Figures 10b and 10d) show increased evidence of dissolution in both the shallow (Figure 10b) and deep (Figure 10d) cores, including increased pore sizes, excessive pitting (shown in the enlarged SEM (Figure 10f) detailing the boxed area of Figure 10d), and in the deeper core indications of intense dissolution are present, including extensive cracking and broken shells (not pictured here). The scale bar is 200 μm.

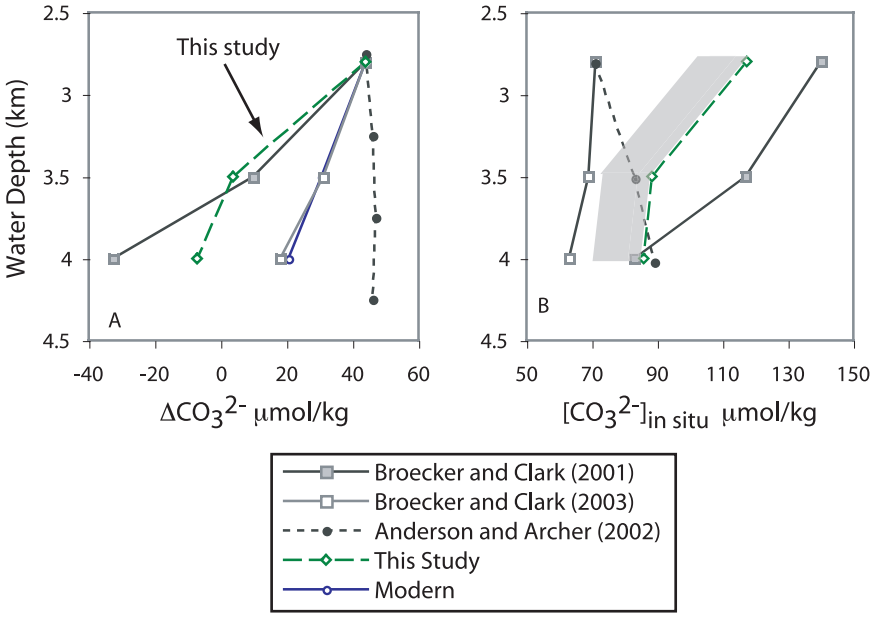

Figure 11. (a) Comparison of the ΔCO_3^{2-} gradient reconstructed from three proxies: Mg/Ca (green dashed line, this study), shell weights (gray solid lines) [*Broecker and Clark*, 2001a and 2003], and assemblage changes (black dashed line) [*Anderson and Archer*, 2002]. As in the previous figure, $\Delta CO_3^{2-} = [CO_3^{2}]_{sat} - [CO_3^{2-}]_{in\ situ}$. For comparison we have normalized all three reconstructions relative to the modern value at the shallowest site. Both the initial shell weight reconstruction [*Broecker and Clark*, 2001a] and Mg/Ca reconstruction decrease with depth, while the reconstruction based on assemblage changes and the more recent shell weight reconstruction [*Broecker and Clark*, 2003] show no change with depth. (b) Comparison of the in situ CO_3^{2-} gradient (i.e., not corrected for changes in carbonate saturation due to depth). The gradient based on assemblage changes increases with depth; the gradient based on Mg/Ca and shell weights [*Broecker and Clark*, 2001a] decreases with depth; and the revised shell weight reconstruction [*Broecker and Clark*, 2003] decreases slightly with depth.

tropical thermocline estimates (although slightly larger than SST estimates) and any shift in carbonate ion content would imply a smaller glacial-interglacial temperature change.

4.6. Comparison of Glacial Reconstructions

[37] We compare our gradient with several other reconstructions from the deep glacial Atlantic (Figure 11). For comparison, we examine differences in both ΔCO_3^{2-} (Figure 11a) and $[CO_3^{2-}]_{in\ situ}$ (Figure 11b). For direct comparison we have calculated the *Broecker and Clark* [2001a, 2003] values using the same $[CO_3^{2-}]_{sat}$ values used in our Mg-derived reconstruction. Our ΔCO_3^{2-} gradient (Figure 11a) is not as steep as the gradient reconstructed by *Broecker and Clark* [2001a] using shell weights but is broadly similar in structure. Both our reconstruction and the shell weight derived reconstruction show steeply decreasing ΔCO_3^{2-} between the shallow and deep cores. The difference between these two reconstructions is that the steep trend extends to the deeper core in the shell weight derived reconstruction, leading to a slightly different conclusion about the deepwater mass structure. The differences between the two reconstructions could reflect an underestimation of the ΔCO_3^{2-} by the Mg-based proxy or an overestimate by the shell-mass proxy. Recognizing that their deepest core yielded very low $[CO_3^{2-}]_{in\ situ}$, *Broecker and Clark* [2001a] suggest that the effect of dissolution in pore waters may produce a steeper relationship between shell mass and $[CO_3^{2-}]_{in\ situ}$. However, it is difficult to invoke this explanation as a cause of differences between our Mg-derived reconstruction and the reconstruction based on shell weights because we use many of the exact same shells used in *Broecker and Clark*'s [2001a] shell weight reconstruction. It may be that one or both of the proxies have a nonlinear response at high dissolution intensities. For example, shell Mg-content may become less sensitive to dissolution after crossing some threshold $[CO_3^{2-}]_{in\ situ}$ value; or, shell weights may rapidly begin to dissolve after crossing some threshold.

[38] *Broecker and Clark* [2003] revised their results in a more recent study using a larger initial shell weight for glacial shells and a modified pressure-normalized loss of shell weight due to

changes in bottom water carbonate ion concentration. Their revised results suggest increased dissolution in the Atlantic during the LGM but do not indicate a shift in water mass configuration. Rather, their revised glacial gradient is identical in shape to the modern gradient with a decrease in carbonate ion concentration during the LGM from the shallow to deep core of 9 μmol/kg, comparable to the modern range of ~5 μmol/kg. In contrast to our results, Broecker and Clark's revised reconstruction (1) does not imply a sharp boundary in water masses between any of the cores and (2) implies a much smaller difference in deep water $[CO_3^{2-}]$ between the shallow and deep cores.

[39] *Anderson and Archer* [2002] reconstruct a depth profile for carbonate saturation state that is fairly constant, or slightly increasing, with water depth. This gradient is inconsistent with our ΔCO_3^{2-} reconstruction as well as qualitative observations of the preservation state of foraminifera from deep Atlantic cores, at least on the Ceara Rise and in the eastern tropical Atlantic. Shells from glacial intervals show visual signs of dissolution, including lack of fine details (Figure 10), increased fragmentation of fragile specimens and, as we observed during sample preparation, shells that crack more easily. This qualitative evidence, in combination with our observations of enhanced Mg loss in glacial shells from our deepest core, suggest that the statistical approach used by *Anderson and Archer* [2002] does not yield an accurate picture of dissolution in the tropical Atlantic. Perhaps the assemblage changes associated with cooler surface waters complicate extracting a robust secondary dissolution signal in the tropics.

[40] Comparison of the reconstructions of the in situ CO_3^{2-} gradient (Figure 11b) lends further insight into the differences among the studies presented above. Our reconstruction is based on the assumption that the entire Mg/Ca change in the shallow core is due to temperature, i.e., we assume no change in CO_3^{2-} the in the shallow core. If we relax this assumption, and attribute the entire Mg/Ca change in the shallow core to dissolution, our values would shift 15 μmol/kg lower, to an in situ CO_3^{2-} of 102 μmol/kg (gray shading, Figure 9b). Further subtracting 9 μmol/kg (our estimated error) yields an in situ CO_3^{2-} of 93 μmol/kg, ~25 μmol/kg higher than either of the *Broecker and Clark* [2003] and the Anderson and Archer reconstructions (~70 μmol/kg). Additional studies are needed to reconcile differences between the different methods of reconstructing deepwater carbonate ion concentration.

4.7. Limitations and Complications in Reconstructing in Situ CO_3^{2-} From Mg/Ca

[41] There are several potential complications with reconstructing $[CO_3^{2-}]_{\text{in situ}}$ from foraminiferal Mg/Ca. One complication is that we assume that no postdepositional dissolution occurs in the sediments. Studies have shown that dissolution in sediment can occur both above and below the calcite saturation horizon due to the respiration of organic matter in sediments, which releases metabolic acids and causes dissolution of calcium carbonate [*Martin and Sayles*, 1996]. However, as *Broecker and Clark* [2001a] note, this is a common limitation to studies deriving $[CO_3^{2-}]_{\text{in situ}}$ from a process controlled by dissolution (e.g., shell weights, assemblages, and fragmentation).

[42] Additional complications arise from the lack of understanding on why increased dissolution decreases the Mg/Ca ratio. For instance, structurally *N. dutertrei* is resistant to dissolution and yet the decrease in the magnitude of magnesium loss is greatest in this species. Additionally, recent studies have shown that the composition of ontogenic and gametogenic calcite varies [*Eggins et al.*, 2003; *Hathorne et al.*, 2003]. These studies also show that layers of calcite precipitated sequentially and in shells with multiple chambers (i.e., *N. dutertrei*) the Mg/Ca in the calcite varies. Shell chemistry may be further complicated in species that migrate in the water column during their lifecycle. For example, *G. sacculifer* appears to add gametogenic calcite at a deeper depth and *N. dutertrei* appears to migrates throughout the water column during its lifecycle [*Fairbanks and Wiebe*, 1980; *Eggins et al.*, 2003]. Layers that calcify in different depths should have different Mg/Ca ratios due to the change in water temperature. Differences in LGM water column structure could complicate our Mg-derived CO_3^{2-} proxy. Our temperature reconstructions, however, imply a comparable water column structure during the LGM at least over the top 75 m of the water column (Figure 4).

5. Conclusions

[43] The Mg/Ca of all three species indicate cooler LGM sea surface (2.4°C lower than modern) and thermocline temperatures (4.2°C lower than modern). These results are generally consistent with estimates of tropical SST changes based on other

proxies. Our down core results confirm differences in the loss of Mg due to dissolution among different species, a difference that has been observed in core top data sets. The Mg/Ca of *G. ruber* and *G. sacculifer* are less affected by dissolution than the thermocline dwelling *N. dutertrei* and are therefore less affected by a shift in the lysocline that may coincide with glacial cycles. The effect of dissolution on the Mg/Ca of *N. dutertrei*, however, is much greater relative to the glacial-interglacial Mg/Ca change due to temperature. To reconstruct thermocline temperatures using this species, cores well above the lysocline should be chosen.

[44] Several factors make *N. dutertrei* useful for reconstructing changes in carbonate ion concentration. First, the Mg-content of *N. dutertrei* is more sensitive to dissolution than the surface dwelling species. Second, their Mg-content is not as sensitive to changes in temperature. Third, *N. dutertrei* are structurally resistant to dissolution, remaining intact in sediment where less robust species suffer from fragmentation and complete dissolution. The accurate reconstruction of the modern ΔCO_3^{2-} gradient, from *N. dutertrei*, demonstrates the utility of this species for paleo-ΔCO_3^{2-} reconstructions.

[45] The ΔCO_3^{2-} reconstruction derived from *N. dutertrei* Mg/Ca presented here indicates a change in the shape of the ΔCO_3^{2-} profile as well as a steeper dissolution gradient on the Ceara Rise during the LGM. The similar $[CO_3^{2-}]_{in\ situ}$ in the middepth and deep cores suggests that these two cores were bathed in the same water mass during the LGM. The amplitude of the $[CO_3^{2-}]_{in\ situ}$ change is consistent with a simple upward shift in the boundary between NADW and AABW, with similar contrasts in $[CO_3^{2-}]_{in\ situ}$ as today. However, evidence of some enhanced glacial dissolution of shells from the shallowest core suggests that the contrast between these two water masses was slightly larger than in the modern ocean. Our gradient is broadly consistent with, although not as steep as, the $[CO_3^{2-}]_{in\ situ}$ reconstruction of *Broecker and Clark* [2001a] lending some support to the utility of both of these proxies.

[46] The approach we detail requires comparison of cores in a single region from multiple water depths. Ideally, cores chosen for a Mg-derived CO_3^{2-} reconstruction should include at least one core located above the lysocline in order to minimize the effect of dissolution on the shallow core temperature reconstruction and constrain the error on the $[CO_3^{2-}]_{in\ situ}$. Alternatively, an independent proxy for sea surface temperature could be used to quantify changes in the Mg/Ca ratio due to temperature independent of the Mg-content of the shells; however, our approach works best with the thermocline dwelling *N. dutertrei*, making an independent temperature reconstruction more challenging. The results from this study suggest comparison of Mg/Ca from multiple cores (multiple depths) from one region could provide constraints on changes in carbonate chemistry in other basins and other time periods.

Acknowledgments

[47] We thank Bill Curry and Dorinda Ostermann of Woods Hole Oceanographic Institute and Wally Broecker and Elizabeth Clark of Lamont-Doherty Earth Observatory, Columbia University, for providing samples from the Ceara Rise. We also thank G. Paradis and David Lea for sample analysis at the University of California, Santa Barbara. Thanks also to Dotti Pak at the University of California, Santa Barbara, for improving the manuscript and to David Lea and David Archer for scientific discussions. Lauren Camp, Fern Gibbons, and Erin Atkinson assisted with cleaning of the samples. Erin Atkinson took the SEM photographs at the University of Chicago with the supervision of Andy Davis.

References

Adkins, J. F., E. A. Boyle, L. Keigwin, and E. Cortijo (1997), Variability of the North Atlantic thermohaline circulation during the last interglacial period, *Nature*, *390*, 154–156.

Adkins, J. F., K. McIntyre, and D. P. Schrag (2002), The salinity, temperature, and $\delta^{18}O$ of the glacial deep ocean, *Science*, *298*, 1769–1773.

Anand, P., H. Elderfield, and M. H. Conte (2003), Calibration of Mg/Ca thermometry in planktonic foraminifera from a sediment trap time series, *Paleoceanography*, *18*(2), 1050, doi:10.1029/2002PA000846.

Anderson, D. M., and D. E. Archer (2002), Glacial-interglacial stability of ocean pH inferred from foraminifer dissolution rates, *Nature*, *416*, 70–73.

Archer, D. E., and E. Maier-Reimer (1994), Effect of deep-sea sedimentary calcite preservation on atmospheric CO_2 concentration, *Nature*, *367*, 260–263.

Archer, D. E., A. Winguth, D. Lea, and N. Mahowald (2000), What caused the glacial/interglacial atmospheric CO_2 cycles?, *Rev. Geophys.*, *38*, 159–189.

Barker, S., and H. Elderfield (2002), Foraminiferal calcification response to glacial-interglacial changes in atmospheric CO_2, *Science*, *297*, 833–836.

Barker, S., T. Kiefer, and H. Elderfield (2004), Temporal changes in North Atlantic circulation constrained by planktonic foraminiferal shell weights, *Paleoceanography*, *19*, PA3008, doi:10.1029/2004PA001004.

Bassinot, F. C., F. Mélières, M. Gehlen, C. Levi, and L. Labeyrie (2004), Crystallinity of foraminifera shells: A proxy to reconstruct past bottom water CO_3^{2-} changes?, *Geochem. Geophys. Geosyst.*, *5*, Q08D10, doi:10.1029/2003GC000668.

Berger, W. (1970), Planktonic foraminifera: Selective solution and the lysocline, *Mar. Geol.*, *8*, 111–138.

Boyle, E. A., and L. Keigwin (1987), North Atlantic thermohaline circulation during the past 20,000 years linked to high-latitude surface-temperature, *Nature*, *330*, 35–40.

Boyle, E. A., and L. D. Keigwin (1985), Comparison of Atlantic and Pacific paleochemical records for the last 215,000 years: Changes in deep ocean circulation and chemical inventory, *Earth Planet. Sci. Lett.*, *76*, 135–150.

Broecker, W. S. (1982), Glacial to interglacial changes in ocean chemistry, *Prog. Oceanogr.*, *11*, 151–197.

Broecker, W. S., and E. Clark (2001a), Glacial-to-Holocene redistribution of carbonate ion in the deep sea, *Science*, *294*, 2152–2155.

Broecker, W. S., and E. Clark (2001b), Reevaluation of the $CaCO_3$ size index paleocarbonate ion proxy, *Paleoceanography*, *16*(6), 669–672.

Broecker, W. S., and E. Clark (2003), Glacial-age deep sea carbonate ion concentrations, *Geochem. Geophys. Geosyst.*, *4*(6), 1047, doi:10.1029/2003GC000506.

Broecker, W. S., and S. Sutherland (2000), Distribution of carbonate ion in the deep ocean: Support for a post-Little Ice Age change in Southern Ocean ventilation?, *Geochem. Geophys. Geosyst.*, *1*(7), doi:10.1029/2000GC000039.

Brown, S. J., and H. Elderfield (1996), Variations in Mg/Ca and Sr/Ca ratios of planktonic foraminifera caused by post-depositional dissolution: Evidence of shallow Mg-dependent dissolution, *Paleoceanography*, *11*(5), 543–552.

Curry, W. B., and D. W. Oppo (2005), Glacial water mass geometry and the distribution of $\delta^{13}C$ of ΣCO_2 in the western Atlantic Ocean, *Paleoceanography*, *20*, PA1017, doi:10.1029/2004PA001021.

Curry, W. B., J. C. Duplessy, L. D. Labeyrie, and N. J. Shackleton (1988), Changes in the distribution of ^{13}C of deep water ΣCO_2 between the last glaciation and the Holocene, *Paleoceanography*, *3*, 317–341.

de Villiers, S. (2003), Dissolution effects on foraminiferal Mg/Ca records of sea surface temperature in the western equatorial Pacific, *Paleoceanography*, *18*(3), 1070, doi:10.1029/2002PA000802.

de Villiers, S. (2004), Optimum growth conditions as opposed to calcite saturation as a control on the calcification rate and shell-weight of marine foraminifera, *Mar. Biol.*, *144*, 45–49.

Dekens, P. S., D. W. Lea, D. K. Pak, and H. J. Spero (2002), Core top calibration of Mg/Ca in tropical foraminifera: Refining paleotemperature estimation, *Geochem. Geophys. Geosyst.*, *3*(4), 1022, doi:10.1029/2001GC000200.

Duplessy, J. C., N. J. Shackleton, R. G. Fairbanks, L. Labeyrie, D. Oppo, and N. Kallel (1988), Deepwater source variations during the last climatic cycle and their impact on the global deepwater circulation, *Paleoceanography*, *3*, 343–360.

Eggins, S., P. D. Deckker, and J. Marshall (2003), Mg/Ca variation in planktonic foraminifera tests: Implications for reconstructing palaeo-seawater temperature and habitat migration, *Earth Planet. Sci. Lett.*, *212*, 291–306.

Elderfield, H., and G. Ganssen (2000), Past temperature and $\delta^{18}O$ of surface ocean waters inferred from foraminiferal Mg/Ca ratios, *Nature*, *405*, 442–445.

Fairbanks, R. G., and P. Wiebe (1980), Foraminifera and chlorophyll maximum: Vertical distribution, seasonal succession, and paleoceanographic significance, *Science*, *209*, 1524–1526.

Fairbanks, R. G., M. Sverdlove, R. Free, P. Wiebe, and A. Be (1982), Vertical distribution and isotopic fractionation of living planktonic foraminifera from the Panama Basin, *Nature*, *298*, 841–844.

Guilderson, T. P., R. G. Fairbanks, and J. L. Rubenstone (2001), Tropical Atlantic coral oxygen isotopes: Glacial-interglacial sea surface temperature and climate change, *Mar. Geol.*, *172*, 75–89.

Hastings, D. W., A. D. Russell, and S. R. Emerson (1998), Foraminiferal magnesium in *Globeriginoides sacculifer* as a paleotemperature proxy, *Paleoceanography*, *13*(2), 161–169.

Hathorne, E. C., O. Alard, R. H. James, and N. W. Rogers (2003), Determination of intratest variability of trace elements in foraminifera by laser ablation inductively coupled plasma-mass spectrometry, *Geochem. Geophys. Geosyst.*, *4*(12), 8408, doi:10.1029/2003GC000539.

Labeyrie, L. D., J. C. Duplessy, J. Duprat, A. Juilletleclerc, J. Moyes, E. Michel, N. Kallel, and N. J. Shackleton (1992), Changes in the vertical structure of the north Atlantic Ocean between glacial and modern times, *Quat. Sci. Rev.*, *11*(4), 401–413.

Lea, D. W., and P. Martin (1996), A rapid mass spectrometric method for the simultaneous analysis of barium, cadmium, and strontium in foraminiferal shells, *Geochim. Cosmochim. Acta*, *60*, 3143–3149.

Lea, D. W., T. Mashiotta, and H. J. Spero (1999), Controls on magnesium and strontium uptake in planktonic foraminifera determined by live culturing, *Geochim. Cosmochim. Acta*, *63*, 2369–2379.

Levitus, S., and T. P. Boyer (1994), World Ocean Atlas, Temperature, NOAA Atlas NESDIS, Natl. Oceanic and Atmos. Admin., Silver Spring, Md.

Lohmann, G. P. (1995), A model for variation in the chemistry of planktonic foraminifera due to secondary calcification and selective dissolution, *Paleoceanography*, *10*, 445–457.

Marchitto, T. M.Jr., D. W. Oppo, and W. B. Curry (2002), Paired benthic foraminiferal Cd/Ca and Zn/Ca evidence for a greatly increased presence of Southern Ocean Water in the glacial North Atlantic, *Paleoceanography*, *17*(3), 1038, doi:10.1029/2000PA000598.

Martin, P. A., and D. W. Lea (1998), Comparison of water mass changes in the deep tropical Atlantic derived from Cd/Ca and carbon isotope records: Implications for changing Ba composition of deep Atlantic water masses, *Paleoceanography*, *13*(6), 572–585.

Martin, P. A., and D. W. Lea (2002), A simple evaluation of cleaning procedures on fossil benthic foraminiferal Mg/Ca, *Geochem. Geophys. Geosyst.*, *3*(10), 8401, doi:10.1029/2001GC000280.

Martin, W. R., and F. L. Sayles (1996), $CaCO_3$ dissolution in sediments of the Ceara Rise, western equatorial Atlantic, *Geochim. Cosmochim. Acta*, *60*, 243–263.

McConnell, M. C., and R. C. Thunell (2005), Calibration of the planktonic foraminiferal Mg/Ca paleothermometer: Sediment trap results from the Guaymas Basin, Gulf of California, *Paleoceanography*, *20*, PA2016, doi:10.1029/2004PA001077.

McKenna, V. S., and W. L. Prell (2004), Calibration of the Mg/Ca of *Globorotalia truncatulinoides* (R) for the reconstruction of marine temperature gradients, *Paleoceanography*, *19*, PA2006, doi:10.1029/2000PA000604.

Mix, A. C., A. E. Morey, N. G. Pisias, and S. W. Hostetler (1999), Foraminiferal faunal estimates of paleotemperature: Circumventing the no-analog problem yields cool ice age tropics, *Paleoceanography*, *14*(3), 350–359.

Moore, J. K., M. R. Abbott, J. G. Richman, and D. M. Nelson (2000), The Southern Ocean at the last glacial maximum: A strong sink for atmospheric carbon dioxide, *Global Biogeochem. Cycles*, *14*, 455–475.

Pak, D. K., D. W. Lea, and J. P. Kennett (2004), Seasonal and interannual variation in Santa Barbara Basin water temperatures observed in sediment trap foraminiferal Mg/Ca, *Geo-*

chem. Geophys. Geosyst., *5*, Q12008, doi:10.1029/2004GC000760.

Pfuhl, H. A., and N. J. Shackleton (2004), Two proximal, high resolution records of foraminiferal fragmentation and their implications for changes in dissolution, *Deep Sea Res., Part I*, *51*, 809–832.

Rosell-Melé, A., E. Bard, K. Emeis, B. Grieger, C. Hewitt, P. J. Müller, and R. R. Schneider (2004), Sea surface temperature anomalies in the oceans at the LGM estimated from the alkenone-$U^{K'}_{37}$ index: Comparison with GCMs, *Geophys. Res. Lett.*, *31*, L03208, doi:10.1029/2003GL018151.

Rosenthal, Y., and G. P. Lohmann (2002), Accurate estimation of sea surface temperatures using dissolution-corrected calibrations for Mg/Ca paleothermometry, *Paleoceanography*, *17*(3), 1044, doi:10.1029/2001PA000749.

Sanyal, A., N. G. Hemming, G. N. Hanson, and W. S. Broecker (1995), Evidence for a higher pH in the glacial ocean from boron isotopes in foraminifera, *Nature*, *373*, 234–236.

Sigman, D. M., and E. A. Boyle (2000), Glacial/interglacial variations in atmospheric carbon dioxide, *Nature*, *407*, 859–869.

Slowey, N. C., and W. B. Curry (1995), Glacial-interglacial differences in circulation and carbon cycling within the upper western North Atlantic, *Paleoceanography*, *10*(4), 715–732.

Spero, H. J., J. Bijma, D. W. Lea, and B. E. Bemis (1997), Effect of seawater carbonate concentration on foraminiferal carbon and oxygen isotopes, *Nature*, *390*, 497–500.

Trend-Staid, M., and W. L. Prell (2002), Sea surface temperature at the Last Glacial Maximum: A reconstruction using the modern analog technique, *Paleoceanography*, *17*(4), 1065, doi:10.1029/2000PA000506.

Volbers, A. N. A., and R. Henrich (2002), Late Quaternary variations in calcium carbonate preservation of deep-sea sediments in the northern Cape Basin: Results from a multiproxy approach, *Mar. Geol.*, *180*, 203–220.

Volbers, A. N. A., and R. Henrich (2004), Calcium carbonate corrosiveness in the South Atlantic during the Last Glacial Maximum as inferred from changes in the preservation of *Globigerina bulloides*: A proxy to determine deep-water circulation patterns, *Mar. Geol.*, *204*, 43–57.